Studying the influence of refrigerant type on thermal efficiency of annular two-phase flows; mass transfer viewpoint

Zahra Baniamerian[†,‡] and Cyrus Aghanajafi

Department of Mechanical Engineering, K.N.T University of Technology, Tehran, Iran
(*Received 23 February 2010 • accepted 24 May 2010*)

Abstract−Many parameters influence the thermal efficiency of two-phase systems; among them, the type of refrigerant employed in two-phase systems is of great importance. Carbon dioxide has been reintroduced as a possible R22 replacement, because of having more heat transfer rate and lower pressure drops, along with better environmental treatment compared with widely-used refrigerants. In the present article carbon dioxide is studied and compared with some thermophysically-different refrigerants from the viewpoint of probability of dry-out occurrence. Dry-out phenomenon in two-phase systems should be avoided as far as possible to prevent sudden drops in heat transfer. Dry-out occurrence is strongly influenced by entrainment mass transfer. In the present study a semi-empirical model is proposed for simulation of entrainment mass transfer in annular flow regime of liquid-vapor in a vertical tube. The significance of entrainment phenomenon in carbon dioxide is compared with that of some other refrigerants to figure out the probability of dry-out occurrence in different refrigerants. It will be demonstrated that CO2 relative to other refrigerants has much lower amounts of entrainment. This issue along with other mentioned advantages shows the prominent effectiveness of carbon dioxide among other conventional refrigerants.

Key words: Annular Flow Regime, Dry Out, Entrainment, Mass Transfer, Refrigerant

INTRODUCTION

Two-phase flow heat transfer characteristics have become an important issue because of their great influence on the performance of cooling systems. Convective boiling heat transfer in channels has been extensively studied. Most of the theoretical and experimental accomplished researches in this area have focused on computation of the heat transfer coefficient [1-6] and some other studies have been devoted to simulation of CHF condition at which dry-out occurs [7-9]. From the design and application viewpoint, avoiding critical heat flux (CHF) is of great importance to achieve the best possible performance of cooling systems. In this regard all the parameters that directly or indirectly affect this phenomenon should be precisely investigated.

Entrainment increases the probability of dry out occurrence, and dry out, in turn, decreases the thermal efficiency of two-phase flows. In annular flow, the liquid film dries out due to evaporation and due to the partial entrainment of the liquid in the form of droplets in the vapor core. At dry out condition the single phase of vapor with some liquid droplets flows in the pipe and since the heat transfer coefficient of vapor is much lower than that of liquid, a sudden drop in heat transfer is experienced.

Entrainment mass transfer as an important issue that strongly influence heat transfer and fluid flow behavior has been studied for many years. Most of the accomplished researches in this field are experimental and have been carried out at restricted operating conditions and on some special fluids like water and some limited number of refrigerants [10-13].

The present study is devoted to simulation of entrainment, based on the physical concepts and mechanism through which it takes place. The contribution of entrainment is then compared with that of evaporation to find how much the entrainment role is significant. The effects of fluid type on the entrainment will be studied at the end.

METHODOLOGY

1. Physical Concept of Entrainment Phenomenon

As vapor flows upon a liquid phase in the annular flow regime, some waves on their interface form and begin to grow (Fig. 1). These
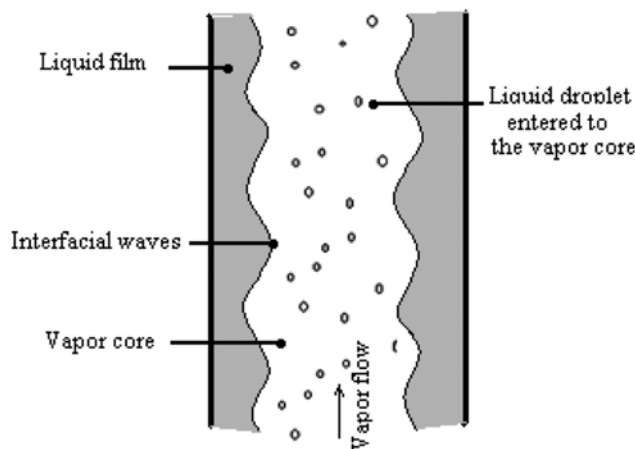

Fig. 1. Schematic of interfacial waves and ripples in a typical annular two-phase flow.

[†]To whom correspondence should be addressed.
E-mail: rr_amerian@yahoo.com
[‡]Present address: Department of Mechanical Engineering, Khaje Nasir Toosi University of Technology, Pardis St., Mollasadra St., Vanaq Sq., Tehran, Iran.
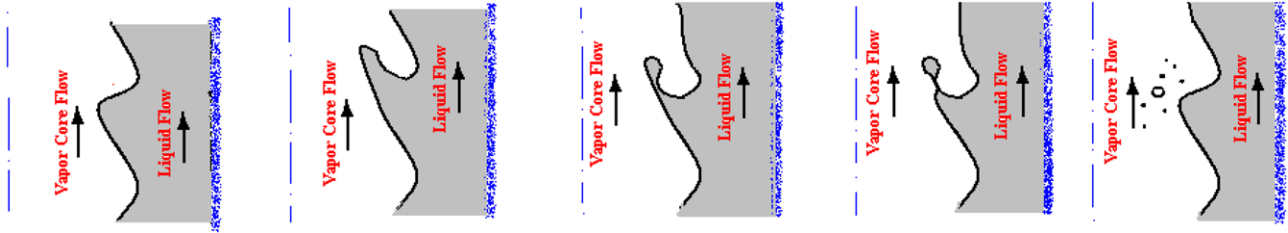
Fig. 2. Undercutting wave crest process by the vapor core flow (follow from left to right).

waves, called interfacial waves, strongly influence the fluid flow. Drag, surface tension, density and velocity difference of fluids flowing next to each other, and boiling phenomenon in the liquid film are the most important issues known to be agents of wave formation at the interface.

For high enough velocities entrainment mass transfer commences due to the effects of interfacial waves. In other words, as the interfacial stress exceeds the retentive force of surface tension, liquid droplets start to transfer in to the vapor core in the annular flow regime.

Undercutting waves crest by the flowing vapor, bursting of bubbles at the interface and impingement of existing droplets of vapor core to the surface of liquid film are some reasonable mechanisms by which this transfer of droplets can be justified. Among those the first mechanism is more associated with interfacial waves and will be of greater interest in this study. Process of undercutting waves crest by the flowing vapor phase is demonstrated in Fig. 2.

There are many studies in the literature concerning with formation of waves, but most of those are not engaged with its consequent influences. As claimed by Thome and Collier [14], interfacial waves of different fluids form in different fluid velocities that directly depend on thermo-physical properties of each fluid. They suggested a critical Re number for the onset of entrainment in annular flow.

Using high-speed cinematography, Woodmansee and Hanratty [15] observed that the principal means of droplet entrainment from a liquid film into vapor core are the rapid acceleration, lifting, and subsequent shattering of ripples on the liquid-vapor interface.

Most entrainment models in the literature are experimental and more dependent on dimensionless groups than on physical potentials of entrainment phenomenon. Despite the consensus on the strong effect of interfacial instabilities on annular entrainment, most available models do not clearly consider this effect. The present study attempts to find the fundamental physics for the entrainment phenomenon. In this regard, entrainment is presumed to be the result of sweeping a fraction of wave crest off into the vapor core as demonstrated in Fig. 2. Regarding this assumption, entrainment rate depends on the volume of liquid removed from the wave crest, wave length, number of waves in the control volume and the wave velocity. The above statement can be simply formulated as [16]:

$$E = \frac{\forall_l \cdot \rho_l \cdot N_w}{t_w \cdot A_{co}} \tag{1}$$

where, E, $\forall_l$, ρ_l, N_w, A_{co} and t_w are entrainment rate, liquid volume removed from each wave crest, liquid density, number of waves, interfacial area and the period of entrainment phenomenon respectively.

Total number of interfacial waves of wavelength, λ in a pipe of length, L and vapor core perimeter, P_{co} can be simply estimated as below:

$$N_w = \frac{P_{co}}{\lambda} \times \frac{L}{\lambda} \tag{2}$$

Interfacial area through which liquid droplets transfer in to the vapor core is:

$$A_{co} = P_{co} \times L \tag{3}$$

And the period of entrainment phenomenon is written as:

$$t_w = \frac{\lambda}{u_g - u_l} \tag{4}$$

Where, u accounts for flow velocity and indices l and g denote liquid and vapor phase respectively. It can be found that determination of interfacial wave characteristics, including wave amplitude, wavelength, velocity and frequency, is the prerequisite for mass transfer calculations. After performing these computations the force balance at the interface should be evaluated to find the exact place on the crest at which the drag force prevails over the retention force and the wave breaks through the point and forms some liquid droplets transferring to the vapor core.

2. Simulation of Interfacial Waves

If a light fluid flows over a layer of a heavier one, their interface becomes unstable when the relative velocity exceeds a critical speed. This instability, known as Kelvin-Helmholtz instability, may occur at the interface of miscible or immiscible fluids, or within a single fluid in the region of a strong density gradient [17]. The Kelvin-Helmholtz instability is of great importance in annular flow heat and mass transfer behavior.

For an unstable annular flow, interfacial waves grow/decay exponentially in their amplitude as time spends. However, experimental observations found interfacial waves of relatively steady amplitudes in typical annular flows. This issue demonstrates that the interfacial waves of common annular flow regimes are of stable condition and can be assumed to have constant amplitude and wave length.

Interfacial waves are assumed to be sinusoidal upon the observations of previous experiments [10,11,18,19]. Upon the recent observations of Alekseenko et al. [20], there are some fine ripples known as secondary waves on the sinusoidal interfacial waves. These ripples have been neglected in the present study since in this study the volume of liquid disjoined from liquid film is our key point and the existence of ripples on the waves does not make effects.

2-1. Wave Length Calculation

From the Kelvin-Helmholtz theory, there is a critical wave length

for which the annular flow experiences a stable set of waves at the interface. This wave length can be calculated through putting a zero value for the imaginary part of the wave propagation velocity. A wave of sinusoidal form traveling at the interface is assumed:

$$y(x,t) = \varepsilon \sin\left(\frac{2\pi}{\lambda}(x - ct)\right) \tag{5}$$

In the above relation, y denotes interfacial wave equation, ε, x, c and t account for wave amplitude, axial coordinate, wave propagation velocity and time, respectively. The wave propagation velocity can be calculated by applying the following relation [17]:

$$c = \frac{(1/2k\delta\rho_l u_l + \rho_g u_g)}{(1/2\rho_l k\delta + \rho_g)} + \frac{i\sqrt{[\sigma k(1/2\rho_l k\delta + \rho_g) - 1/2\rho_l\rho_g k\delta(u_g - u_l)^2]}}{(1/2\rho_l k\delta + \rho_g)} \tag{6}$$

Where, $k=2\pi/\lambda$ is the wave number. δ and σ are representative of liquid film thickness and surface tension. The real and imaginary parts of the wave propagation velocity (c_R and c_I, respectively) are:

$$c_R = \frac{1/2k\delta\rho_l u_l + \rho_g u_g}{1/2\rho_l k\delta + \rho_g}$$

$$c_I = \pm\frac{\sqrt{[\sigma k(1/2\rho_l k\delta + \rho_g) - 1/2\rho_l\rho_g k\delta(u_g - u_l)^2]}}{1/2\rho_l k\delta + \rho_g} \tag{7}$$

By exerting the condition for neutrally stable waves ($c_I=0$), the wave length can be written as:

$$\lambda = \frac{2\pi}{(u_g - u_l)^2(\rho_g/\sigma) - (2\rho_g/\rho_l\delta)} \tag{8}$$

2-2. Wave Amplitude Calculation

The correlation of Glormes and Ishii is employed in this study for computing interfacial waves' amplitude. Glormes and Ishii applied the shear flow methodology to simulate wave propagation with respect to liquid film flow [21]. They suggested the following equation to obtain the wave amplitude:

$$\varepsilon = C_w\mu_l\frac{u_l}{\tau_i} \tag{9}$$

where μ_l and τ_i are representative of liquid viscosity and interfacial shear stress, respectively. C_w is a dimensionless parameter which is defined as the following.

$$N_\mu = \frac{\mu_l}{\left(\rho_l\sigma\left[\frac{\sigma}{g\Delta\rho}\right]^{0.5}\right)^{0.5}} \tag{10}$$

$$\begin{aligned} C_w &= 0.0283N_\mu^{-0.8} &\text{for } N_\mu \leq 0.0667 \\ C_w &= 0.247 &\text{for } N_\mu > 0.0667 \end{aligned} \tag{11}$$

N_μ in the above correlation is the viscosity number, g is the gravitational acceleration, and $\Delta\rho$ is the liquid and vapor densities difference.

Wave length and amplitude is computed up to this part of simulation. Now the point at which the wave crest will be disjoined should be calculated to obtain the exact volume of liquid removed from the liquid at the interface. This point is obtainable through a force analysis on the waves.
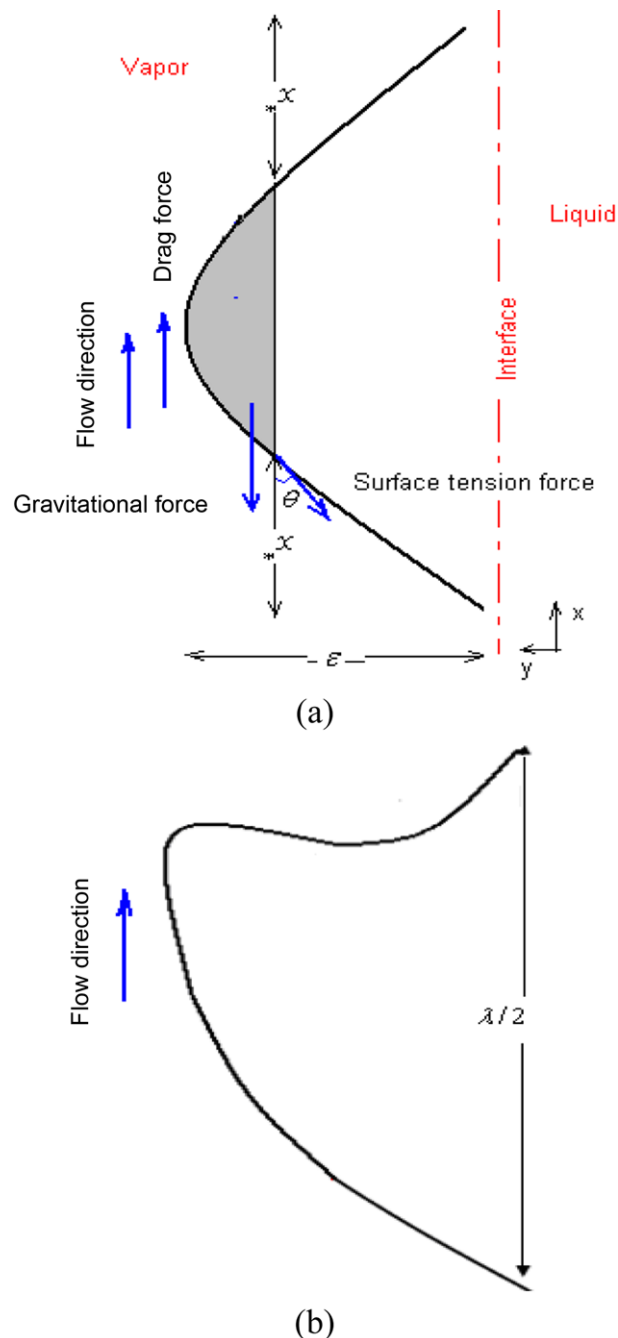

Fig. 3. (a) Forces act on a typical interfacial wave, (b) deformed shape of wave in flow.

2-3. Force Balance on Interfacial Waves

The force balance on the wave is applied to find the disjoining point of the wave. Forces which act on a typical wave are shown in Fig. 3(a). As demonstrated there, the surface tension force is assumed to exert just on the wave front because the wave usually flatten in the rear to experience the least possible surface tension force [16].

As demonstrated in Fig. 3(a), the exerted forces on the crest include interfacial drag, surface tension force and gravity. At this stage, the mentioned forces are calculated individually.

2-3-1. Interfacial Drag

The first considered force is the interfacial drag and is of follow-

ing form:

$$F_D = \frac{1}{2}f_i\rho_{co}A_{co}u_{co}^2 \tag{12}$$

, where F_D and f_i account for interfacial drag and interfacial friction factor, respectively. ρ_{co} and u_{co} are the homogeneous density and velocity of vapor core.

Interfacial shear stress is computed in the work of Holowach and Hochreiter [16], applying liquid density and velocity instead of those of vapor core. In the present study, applying interfacial shear stress in the form of Eq. (12) results in better consistency with experimental results of similar conditions. Therefore, vapor core characteristics are applied to obtain interfacial shear stress.

Interfacial friction factor, f_i, can be obtained by applying the correlation of Wongwises and Kongkiatwanitch that is for the case of two-phase flows with entrainment mass transfer taking place [22]:

$$f_i = 17.172(Re_g)^{-0.768}(\delta/D)^{-0.253}$$
$$Re_g = \frac{\rho_g u_g(D-2\delta)}{\mu_g} \tag{13}$$

where Re_g and D account for the vapor core Reynolds Number and the pipe diameter, respectively.

The area on which drag force acts can be calculated as:

$$A_{disjoining} = \int_{x^*}^{\lambda/2-x^*} \varepsilon\sin(kx)dx - [\varepsilon - \varepsilon\sin(kx^*)]\left(\frac{\lambda}{2} - 2x^*\right) \tag{14}$$

Where, x^* demonstrates axial position of wave disjoining point (Fig. 3a).

2-3-2. Gravitational Force

The volume of the liquid disjoined from the wave should be calculated to obtain the gravitational force. This volume can be computed by applying disc integration over the limits demonstrated in Fig. 3(a). The volume is written in terms of axial coordinate of the disjoining point [16]:

$$k^* = 2\pi x^*/\lambda \tag{15}$$

$$\forall_l = \frac{\varepsilon\lambda^2}{4\pi}\left[\frac{-2 + 2\sin k^* + 2(1-\sin^2 k^*)^{1/2}}{\cos^{-1}(\sin k^*) - \sin k^*(\cos^{-1}(\sin k^*))^2}\right]$$

Then the gravitational force can be achieved:

$$F_g = \rho_l\forall_l g \tag{16}$$

2-3-3. Surface Tension Force

The surface tension force on the front of the wave is calculated through the following correlation:

$$F_\sigma = \sigma K_{crest,avg}A_\sigma \tag{17}$$

Where, σ, $K_{crest,avg}$, A_σ, account for surface tension, average curvature of the wave crest, and the effective area on which the surface tension force acts, respectively.

The curvature of the wave of sinusoidal form can be calculated using the following relation [23]:

$$K_{crest,avg} = |-(k^2\varepsilon)\sin(kx)|/[1+((k)\cos(kx))^2]^{3/2} \tag{18}$$

It is assumed for simplicity that the area on which the surface

tension force acts is a semi-circle of diameter $(\lambda/2-2x^*)$. This assumption is based on the wave deformation [16].

$$A_\sigma = \frac{\pi}{8}(\lambda/2 - 2x^*)^2 \tag{19}$$

The surface tension force acts tangentially to the wave profile, and since in this study the sinusoidal profile is assumed for the wave, the angle, θ shown in Fig. 3(a) is:

$$\theta = \tan^{-1}(k\varepsilon\cos(kx)) \tag{20}$$

Substituting relations (18-20) into Eq. (17) results in:

$$F_\sigma = (\pi/8)\sigma\left\{\frac{-k^2\varepsilon\sin(kx^*)}{[1+(k\cos(kx^*))^2]^{3/2}}\right\}(\lambda/2 - 2x^*)^2 \tag{21}$$

As mentioned before, the forces which act on wave profile are surface tension, drag and gravity. The point at which these forces balance is assumed the disjoining point of wave, since after this point the drag force prevails over the retentive force of surface tension and results in sweeping a little part of the wave off and transferring in to the vapor core. The exact coordinate of the disjoining point can be achieved through applying a force balance on the wave:

$$F_D + F_\sigma - F_g = 0 \tag{22}$$

Substituting the value of each force in the above relation results in an implicit equation with a single unknown of x^* that can be solved by trial and error method.

At this stage, all the variables in Eq. (1) have been calculated. It should be noted that the computed value result from Eq. (1) is the maximum value of the entrainment and it isn't necessarily equal to the real entrainment rate which can be measured through experiments. This issue is the result of returning a little fraction of the swept-off wave into the liquid film again because of prompt acceleration of flow in the vapor core. On the other hand, some empirical correlations have been employed during calculation of friction factor and wave amplitude that may exert some errors in our model. Therefore, Eq. (1) should be modified by utilizing a correction factor. To obtain an appropriate correction factor, we have applied results of Utsuno et al.'s experiment [24]. The correction factor is of the following form:

$$CF = 2.5\left(\frac{\rho_g}{\rho_l}\right)^4\left(\frac{1}{\sigma}\right) \tag{23}$$

Therefore, the final form of the entrainment rate correlation will be:

$$E = 2.5\left(\frac{\rho_g}{\rho_l}\right)^4\frac{\forall_l\cdot\rho_l\cdot(u_g-u_l)}{\lambda^3\sigma} \tag{24}$$

The tube is assumed to be warmed up by constant and uniform heat flux similar to the condition applied in experiment of Utsuno et al. [24]. The experiment of Utsuno et al. was accomplished in the pressure range of $3<p<9$ Mpa and Reynolds number range of $5.4\times10^3<Re<3.5\times10^5$. The exerted heat flux in their set of experiments varied from 0.33 to 2 MW/m^2.

The most sensible contribution of mass transfer in two-phase flows is evaporation. Therefore, evaporation can be a good criterion for evaluation of other mass transfer contributions. Evaporation rate is

estimated through the following relation:

$$\dot{m}_{evap} = \frac{q^{\parallel}}{h_{fg}} \qquad (25)$$

In the present study the necessity of considering entrainment mass transfer contribution is evaluated. It is worth introducing a dimensionless factor, named mass transfer ratio, which represents the ratio of entrainment mass transfer to the evaporation contribution.

$$\text{mass transfer ratio} = \frac{m_{en}}{m_{ev}} \qquad (26)$$

RESULTS AND DISCUSSION

A computer program is written in Matlab programming environment to calculate the exact fraction of liquid that is cut off by the shearing force of high-speed flowing vapor at the pipe core. The proposed correlation for entrainment is compared with some empirical correlations and deviations are tabulated and shown in Table 1. Most of the available empirical correlations are obtained from experiments on water as working fluid; therefore, thermo physical characteristics of water are employed in Eq. (24) to achieve an acceptable comparison between the present and other available models.

Entrainment rate has made dimensionless through dividing by total mass flow rate and named "entrainment fraction," e.

$$e = \frac{E}{G} \qquad (27)$$

Variation of entrainment fraction via mass flow velocity is plotted for four thermo-physically different fluids and depicted in Fig. 4. It is found that an increment in mass flow velocity increases the amount of entrainment. To justify this phenomenon, the influence of mass velocity and surface tension, as Weber Number, is evaluated on the interface wave amplitude and wavelength and displayed in Figs. 5 and 6, respectively. Since the interfacial wave amplitude and wave-
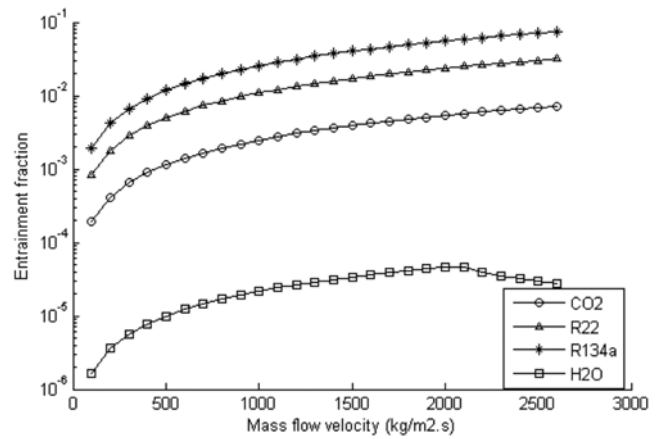

Fig. 4. Variation of entrainment fraction against mass flow velocity; comparison between CO2, R22, R134a and H2O.

length are directly related to the entrainment rate, simulation results of the present study are compared with experimental observations of Sawant et al. [28]. The flow and physical conditions of the present problem are set to those of Sawant et al.'s experiment to have an applicable comparison between the results. It seems that increasing mass velocity decreases wave amplitude and wavelength. The first leads to a decrease in entrainment rate, while the second increases the entrainment contribution through increasing the total number of waves. Results of computer program demonstrate that the second issue is more effective than the first one.

As shown in Fig. 4, the entrainment contribution of mass transfer in carbon dioxide is much less than that of R22 and R134a, while water has the least entrainment contribution among other considered fluids. This issue is due to specific thermo-physical characteristics of water and carbon dioxide that make them different from other refrigerants.

Table 1. Comparison between empirical correlations of entrainment rate and the suggested correlation

Reference	Working fluid	Correlation of entrainment	Mean error*	Average error**
Ishii-Mishima [13]	Water-air	$E = G(1-x)\tanh(7.25 \times 10^{-7} Re_l^{0.25} We_g^{1.25})$ $We_g = \rho_g j_g^2 d / \sigma (\Delta \rho / \rho_g)^{1/3}$	1.5%	1.5%
Hewitt and Whalley [25]	Water-air	$Re_\infty = \exp(5.8504 + 0.4249(\mu_g/\mu_l)\sqrt{\rho_l/\rho_g})$ if $Re_l < Re_\infty$ E=0 if $Re_l > Re_\infty$ $E = 5.75 \times 10^{-5} \alpha_g \rho_g u_g [(Re_l - Re_\infty)^2 (\mu_l^2/d\sigma)\rho_l/\rho_g^2]^{0.316}$	0.5%	−0.1%
Sawant [13]	Water-air	$Re_{film} = 250 \log Re_l - 1265$, $We_g = \rho_g j_g^2 d / \sigma ((\rho_l - \rho_g)/\rho_g)^{0.25}$ $E = G(1-x)(1 - Re_{film}/Re_l)\tanh(2.31 \times 10^{-4} \times Re_l^{-0.35} We_g^{1.25})$	15%	15%
Schadel et al. [26]	Water-air	$Re_\infty = \exp(5.8504 + 0.4249(\mu_g/\mu_l)\sqrt{\rho_l/\rho_g})$ if $Re_l < Re_\infty$, E=0 if $Re_l > Re_\infty$ $E = 1.175 \times 10^{-4} u_g u_l (Re_l - Re_\infty)\sqrt{\rho_l/\rho_g}$	5.5%	−4.3%
Okawa et al. [27]	Water-steam	$f_i = 0.005(1 + 300\delta/d)$ $E = 4.79 \times 10^{-4} (\rho_l/\rho_g)^{0.111} \rho_l \rho_g f_i j_g^2 \delta/\sigma$	2.1%	2.1%
Ueda [12]	Alcohol-air	$U = (\tau/\sigma_l)(\alpha_l \nu_l/\sigma_l)^{0.6}$ $E = 3.54 \times 10^{-3} U^{0.57}$	4.8%	4.8%
Utsuno-Kaminaga [24]	water-Steam	$E = G(1-x)\tanh(0.16 Re_l^{0.16} We_g^{0.08} - 1.2)$ $We_g = \rho_g j_g^2 d / \sigma (\Delta \rho / \rho_g)^{1/3}$	0.84%	−1.28%

*Mean error $= \dfrac{1}{N} \sum_{i=1}^{N} \dfrac{|E|_{present\ model} - E|_{experiment}}{E|_{experiment}} \times 100\%$

**Average error $= \dfrac{1}{N} \sum_{i=1}^{N} \dfrac{|E|_{present\ model} - E|_{experiment}}{E|_{experiment}} \times 100\%$
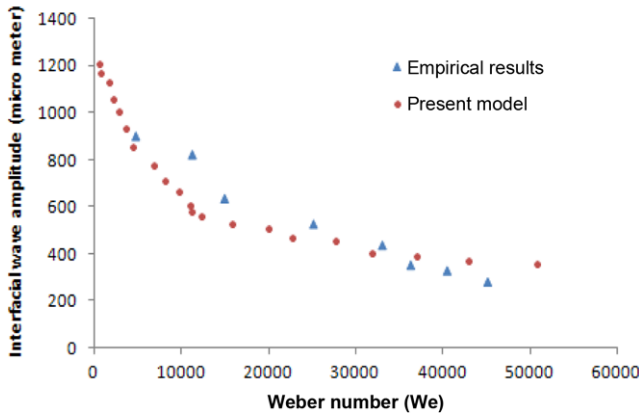
Fig. 5. Variation of interfacial waves amplitude against Weber number; comparison between experiment of Sawant et al. [28] and the present model ($We = \rho_g j_g^2 d/\sigma((\rho_l - \rho_g)/\rho_g)^{1/3}$ where j_g is superficial velocity).
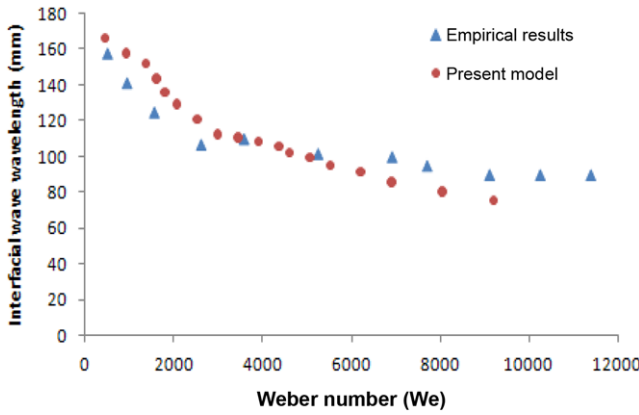

Fig. 6. Variation of interfacial waves wavelength against Weber number; comparison between experiment of Sawant et al. [28] and the present model ($We = \rho_g j_g^2 d/\sigma((\rho_l - \rho_g)/\rho_g)^{1/3}$ where j_g superficial velocity).
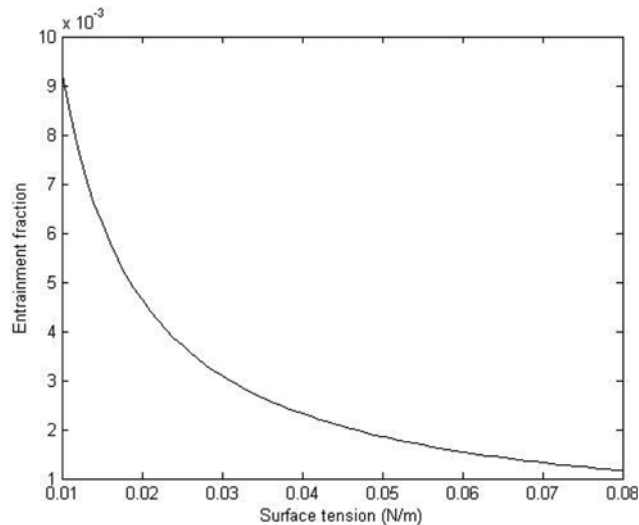

Fig. 7. Variation of entrainment fraction against surface tension.

Variation of entrainment fraction via surface tension changes is plotted and shown in (Fig. 7). It is found that the amount of entrainment decreases with increasing the fluid surface tension. Increasing the fluid surface tension increases the amplitudes of waves propagating at the interface, which in turn increases the entrainment rate potentially (Fig. 5). On the other hand, wavelength increases with surface tension (Fig. 6), which results in a decrement in the number of interfacial waves. When interfacial waves increase in amplitude they are more vulnerable of being cut off by vapor core and a larger amount of liquid enters through the vapor core. Results display that decrease in number of waves prevails over the increase in wave amplitude and at last decreases the entrainment rate with the fluid surface tension.

The other parameter which has been considered in this study is the effect of pipe diameter. In pipes of larger diameter the entrainment fraction is larger than that of smaller ones. Variation of entrainment rate in different pipe diameters is depicted in Fig. 8. It seems that after some diameters, further increment in pipe diameter does not considerably affect entrainment mass transfer.

Variation of mass transfer ratio against wall heat flux is shown in Fig. 9. It can be found from the figure that mass transfer ratio, representing the contribution of entrainment relative to evaporation, takes values that can be hardly ignored. These values emphasize
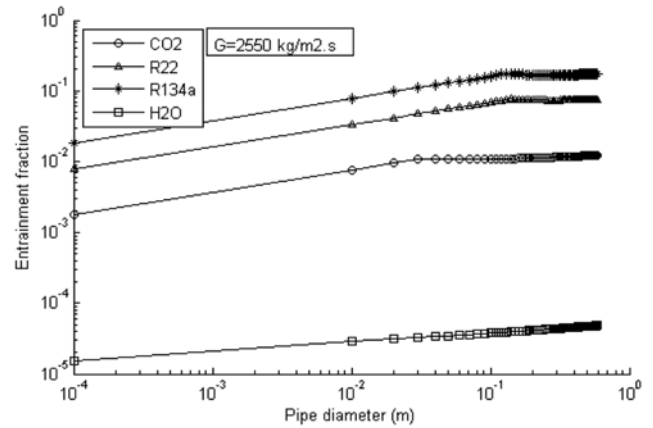

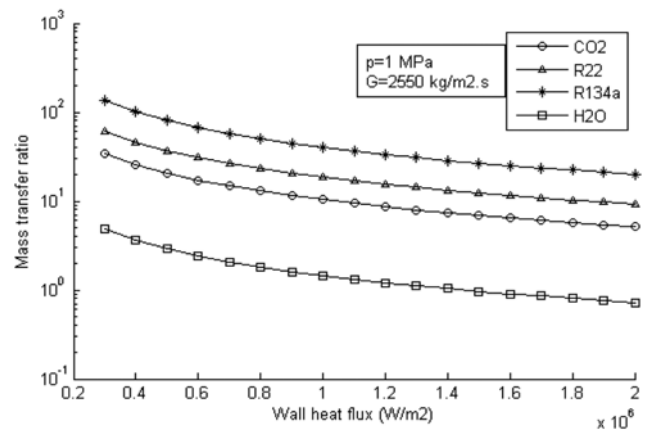**Fig. 8.** Variation of entrainment fraction against pipe diameters.

Fig. 9. Variation of mass transfer ratio against wall heat flux; comparison between CO2, R22, R134a and H2O.

the necessity of considering the effect of entrainment contribution in heat and mass transfer simulation of annular two-phase flows.

It seems that entrainment constitutes a considerable contribution of mass transfer in carbon dioxide, R22 and R134a, while the amount of entrainment mass transfer is less for water in comparison with the other three fluids.

CONCLUSION

Four thermophysically different fluids are considered in this study to be evaluated from the viewpoint of their entrainment mass transfer contribution in annular flow regimes. Results have shown the significant contribution of entrainment in all fluids.

Entrainment contribution of mass transfer is compared with the evaporation contribution and found in similar or at some situations higher order than it. This issue signifies the necessity of considering entrainment in simulations of fluid flow and heat transfer of annular two-phase flows. Therefore, a general entrainment correlation is of great worth. Most of the available correlations of entrainment in the open literature are experiment-based, which have been derived for a specific fluid in special conditions and cannot be generally applied in other situations. In the present study a semi-empirical correlation based on the strong fundamentals of entrainment phenomenon is developed which well satisfies the empirical correlations.

Entrainment fraction is calculated for three popular refrigerants (CO_2, $R134a$ and $R22$) and for water. Comparison between the magnitude of entrainment fraction at different conditions for the four considered fluids shows that CO_2 has lower entrainment fraction compared with other considered refrigerants and water has the minimum contribution of entrainment among all considered fluids. The lower amount of entrained droplets results in lower probability of dry-out occurrence, which in turn increases the efficiency of the cooling system.

REFERENCES

1. W. Qu and I. Mudawar, *Int. J. Heat Mass Transfer*, **46**, 2755 (2003).
2. W. Qu and I. Mudawar, *Int. J. Heat Mass Transfer*, **46**, 2773 (2003).
3. T. Chen and S.V. Garimella, *Int. J. Multiphase Flow*, **32**, 957 (2006).
4. D. S. Wen, Y. Y. Yan and D. B. R. Kenning, *J. App. Therm. Eng.*, **24**, 1207 (2004).
5. W. Cui, L. Li, M. Xin, T. C. Jen, Q. Chen and Q. Liao, *Int. J. Heat Mass Transfer*, **49**, 2851 (2006).
6. D. Brutin and L. Tadrist, *Int. J. Heat Mass Transfer*, **47**, 2365 (2004).
7. W. Qu and I. Mudawar, *Int. J. Heat Mass Transfer*, **47**, 2045 (2004).
8. W. Yu, D. M. France, M. W. Wambsganss and J. R. Hull, *Int. J. Multiphase Flow*, **28**, 927 (2002).
9. M. Kureta and H. Akimoto, *Int. J. Heat Mass Transfer*, **45**, 4107 (2002).
10. L. Pan and T. J. Hanratty, *Int. J. Multiphase Flow*, **28**, 363 (2002).
11. J. R. Barbosa, G. F. Hewitt, G. Konig and S. M. Richardson, *Int. J. Multiphase Flow*, **28**, 943 (2002).
12. I. Kataokaa, M. Ishii and A. Nakayama, *Int. J. Heat & Mass Transfer*, **43**, 1573 (2000).
13. P. Sawant, M. Ishii and M. Mori, *J. Nucl. Eng. Design*, **238**, 1342 (2008).
14. J. G. Collier and J. R. Thome, Convective boiling and condensation, Clarendon Press, Oxford (1996).
15. D. Woodmansee and T. Hanratty, *J. Chem. Eng. Sci.*, **24**, 299 (1969).
16. M. J. Holowach and F. B. Hochreiter, *Int. J. Heat Fluid Flow*, **23**, 807 (2002).
17. G. F. Hewitt and N. S. Hall-Taylor, Annular two-phase flow, Pergamon Press, Oxford (1970).
18. P. Lee and V. S. Garimella, *Int. J. Heat Mass Transfer*, **51**, 789 (2008).
19. S. Vashisth and K. D. Nigam, *J. Chem. Eng. Processing: Process Intensification*, **48**, 452 (2008).
20. S. Alekseenko, V. Antipin, A. Cherdantsev, S. Kharlamov and D. Markovich, *J. Phys. Fluids*, **21**, 061701 (2009).
21. L. W. Zhao, S. G. Kamiel and F. Z. Zhen, *J. Technol.*, **15**, 19 (2004).
22. S. Wongwises and W. Kongkiatwanitch, *Int. Commun. Heat Mass Transfer*, **28**, 3, 323 (2003).
23. D. A. Thomas, Modern geometry, Cole Publishing Co., California (2002).
24. H. Utsuno and F. Kaminaga, *J. Nucl. Sci. Technol.*, **35**, 9, 643 (1998).
25. G. F. Hewitt and P. B. Whalley, *UKAEA Report AERE-9187* (1978).
26. S. A. Schadel, G. W. Leman, J. L. Binder and T. J. Hanratty, *Int. J. Multiphase Flow*, **16**, 363 (1990).
27. T. Okawa, A. Kotani, I. Kataoka and M. Naito, *J Nuc. Sci. Technol.*, **40**, 388 (2003).
28. P. Sawant, M. Ishii, T. Hazukub, T. Takamasab and M. Moric, *J. Nucl. Eng. Design*, **238**, 3528 (2008).